

Communication

A 32-Bit Single Quadrant Angle-Controlled Chipless Tag for Radio Frequency Identification Applications

Muhammad Noman¹, Usman A. Haider¹, Hidayat Ullah¹ , Farooq A. Tahir^{1,*}, Hatem Rmili^{2,3} and Ali I. Najam⁴ 

- ¹ Research Institute for Microwave and Millimeter-Wave Studies, School of Electrical Engineering and Computer Science, National University of Sciences and Technology, Islamabad 44000, Pakistan; munoman.msee18seecs@seecs.edu.pk (M.N.); uhaider.msee18seecs@seecs.edu.pk (U.A.H.); hidayat.ullah@seecs.edu.pk (H.U.)
- ² K.A. CARE Energy Research and Innovation Center, King Abdulaziz University, Jeddah 21589, Saudi Arabia; hmrmili@kau.edu.sa
- ³ Electrical and Computer Engineering Department, Faculty of Engineering, King Abdulaziz University, Jeddah 21589, Saudi Arabia
- ⁴ National Electronics Complex of Pakistan, Islamabad 44000, Pakistan; alimranajam@gmail.com
- * Correspondence: farooq.tahir@seecs.edu.pk

Abstract: A 32-bit chipless RFID tag operating in the 4.5–10.9 GHz band is presented in this paper. The tag has a unique multiple-arc-type shape consisting of closely packed 0.2 mm wide arcs of different radii and lengths. The specific tag geometry provides multiple resonances in frequency domain of an RCS plot. A frequency domain coding technique has also been proposed to encode the tag's RCS signature into a 32-bit digital identification code. The tag has an overall dimension of 17.9×17.9 mm², resulting in a high code density of 9.98 bits/cm² and spectral efficiency of 5 bits/GHz. The proposed tag is built on a low loss substrate bearing a very small footprint, thereby making it extremely suitable for large-scale product identification purposes in future chipless RFID tag systems.



Citation: Noman, M.; Haider, U.A.; Ullah, H.; Tahir, F.A.; Rmili, H.; Najam, A.I. A 32-Bit Single Quadrant Angle-Controlled Chipless Tag for Radio Frequency Identification Applications. *Sensors* **2022**, *22*, 2492. <https://doi.org/10.3390/s22072492>

Academic Editor: Jordi Bonache

Received: 17 February 2022

Accepted: 10 March 2022

Published: 24 March 2022

Publisher's Note: MDPI stays neutral with regard to jurisdictional claims in published maps and institutional affiliations.



Copyright: © 2022 by the authors. Licensee MDPI, Basel, Switzerland. This article is an open access article distributed under the terms and conditions of the Creative Commons Attribution (CC BY) license (<https://creativecommons.org/licenses/by/4.0/>).

Keywords: chipless RFID; product identification; miniaturized; barcode; future systems; IoT

1. Introduction

Optical barcode technology has been used for decades now for the identification, monitoring, reading, and tracking of items in various scenarios [1]. The barcode technology is low cost and reliable; however, the latest developments in communications, computing, and automated systems have raised concerns about the limitations of optical barcode systems. These limitations include primarily the inevitable line of sight (LoS) and strict human–machine interface (HMI) requirements. Furthermore, barcode technology has low security and is short ranged. These limitations can be overcome by using wireless radio frequency identification (RFID) [2]. An RFID system uses a transceiver system and an electronic tag to identify a target item. Applications of RFID include shopping products, cargo items, employee's card reading, vehicle identification, etc. In the near future, it is expected that billions of various different products will use RFID tags [3].

An RFID system provides higher security, longer range, high data capacity, and automated operation as compared to the existing optical barcode systems. The tag used in RFID system are of two types: (1) with on-board electronics and (2) without any electronics. The latter being called a chipless RFID tag and is preferred over the former due to its extremely low cost. The chipless RFID is, therefore, under great focus in research community so that it can be enabled to be used in future product identification systems. Since a chipless RFID (CRFID) tag does not use any onboard electronics, the data encoding becomes quite a challenge. Various encoding schemes have been proposed for CRFID systems, out of

which four techniques are very prominent [4]. These are: (1) the Time-domain technique, (2) the Frequency-domain technique, (3) the Spatial-domain technique, and (4) the Hybrid technique [5–14]. The frequency domain technique works on backscattering phenomena in which a transmitted wave reflects from a metallic tag and its radar cross-section (RCS) is computed. The RCS contains encoded information about the tag in question. Several CRFID tags based on these frequency domain (FD) techniques have been proposed [15–35] to cope with challenges such as: code density, spectral efficiency, conformability, and cost.

Recently published FD-based CRFID tags are mostly based on closed loop resonators, such as [23], which is an elliptically shaped tag having a code density of 2.74 bits/cm² and a spectral efficiency of 0.83 bits/GHz operating in 3.5–15.5 GHz band. A trefoil-shaped tag of [24] operating in 5.4–10.4 GHz band bears an overall size of 13.55 × 13.55 mm². This tag has a code density of 5.44 bits/cm² and spectral efficiency of 2 bits/GHz. Similarly, a butterfly [25] and kite-shaped [26] tags with high bit densities of 5.1 and 5.44 bits/cm² respectively were presented. Both tags operate in 4.7–10 GHz and attain a low-spectral efficiency of 2 bits/GHz. These tags [23–26] have high bit densities due to their compact sizes and complex structures; however, they compromise their bit spectral efficiencies on the other hand.

Open-loop-resonator-based CRFID tags [27–35] have also been reported recently. For example, an 8-bit L shaped tag presented in [27] has a code density of 4 bits/cm² and spectral efficiency of 5.33 bits/GHz. Semi-Elliptical Shaped tag in [28] provides a code density of 4.7 bits/cm² and low spectral efficiency of 1.68 bits/GHz. A dipole-based tags with capacitive loading [29] provides high spectral efficiency of 12.5 bits/GHz, but it has very low code density of 1.77 bits/cm². This is because of its very large size of 16.7 × 67.8 mm². An 8-bit orientation independent circular ring slot-based tag is presented in [30]. The tag has a large area of 60.84 mm² operating in 6–13 GHz that results in very low code density and spectral efficiency of 3.26 bits/cm² and 1.14 bits/GHz, respectively. Similarly, large size tags of [31,32] also results in very low bit densities. For example, coupled-line micro-strip-resonator-based tag [31] has a size of 60.3 × 11 mm² and a code density of 1.1 bits/cm². A rectangular ring slot-based resonator [32] has a simple design with a size of 35 × 35 mm², providing a very low 0.98 bits/cm² code density and a 1.9 bits/GHz of spectral efficiency.

In this paper, a miniaturized 17.9 × 17.9 mm² novel 32-bit chipless RFID tag on an ultra-thin 0.127 mm substrate is presented. The tag geometry is designed such that the length of the resonators is angle-controlled in a single quadrant, rendering the tag an efficient design in respect with radar cross-section (RCS) responses with multiple angle-controlled resonances. Furthermore, the desired frequency spectrum is intelligently utilized resulting in high spectral efficiency. The novelty in the proposed design is two folds: (1) an angle-based geometry to intelligently produce a desired tag ID and (2) a customized encoding technique with unique categorization of frequency-RCS sample space.

2. Tag Design

2.1. Theoretical Tag Design and Coding Scheme

The proposed tag is built upon a thin 0.127 mm Roger's RT Duroid 5880 substrate with $\epsilon_r = 2.2$ and $\tan\delta = 0.0009$. The theoretical geometry of the tag is shown in Figure 1, with an overall dimension of $L_{\text{sub}} \times W_{\text{sub}}$ mm².

The top side of tag consists of 'N' number of arcs of arbitrary lengths ' L_N '. All these arcs exist in the first quadrant of a 2-dimensional plane having a radius R_N . Each arc length starts at 0° from x-axis and terminate at an angle θ_N . All arcs have a width of 'w' are separated by a distance 'g'. The back side of proposed tag does not contain any copper layer and remains empty. The idea behind using multiple arcs of various lengths is that each arc will produce an RCS resonance in the frequency domain, thereby enabling the realization of a single logical bit.

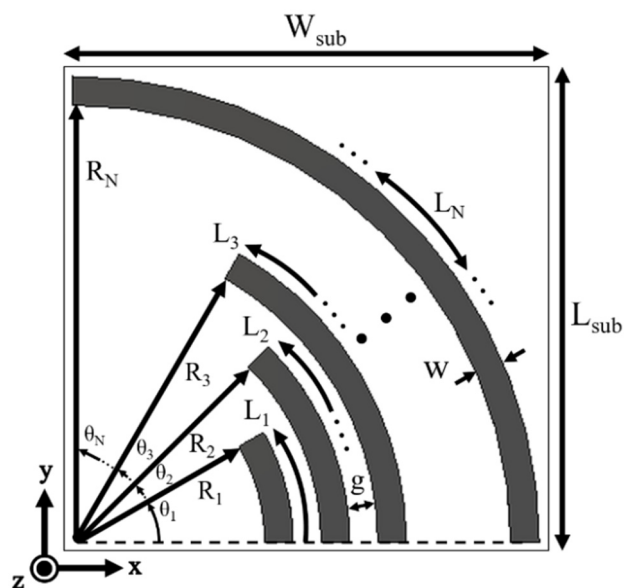


Figure 1. Proposed theoretical tag design.

The coding scheme used for the proposed tag is frequency domain coding, for which the spectral allocation is shown in Figure 2a. The operating band chosen for this particular tag design is 4.5 to 10.9 GHz. A frequency slot of 150 MHz has been designated to indicate the existence of a valid logical bit, known as a ‘bit slot’. Hence, there are a total of ‘N’ bit slots within the operating band. Each ‘bit slot’ is separated by a ‘guard band’ of 50 MHz. The guard bands will be used to separate the identification of a true and a false bit-reading. The most significant bit is chosen to be ‘bit slot 1’, whereas ‘bit slot N’ is the least significant bit in an N-bit ID code. A bit slot start frequency is indicated by ‘fa’ and its stop frequency by ‘fb’ with a subscript ‘N’ showing its bit-position.

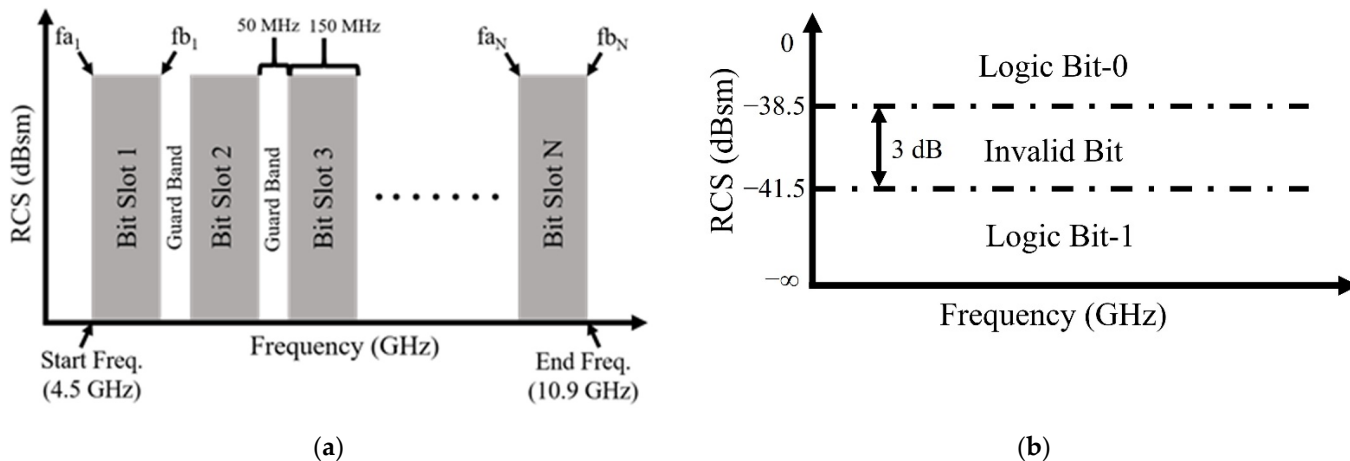


Figure 2. (a) Spectral allocation for the proposed tag; (b) RCS magnitude allocation for the proposed tag.

To further enhance bit-reading mechanism, the vertical RCS axis has been divided into three main regions: (1) a valid logic bit-0 region, (2) a valid logic bit-1 region, and (3) an invalid bit region. This division of RCS magnitude is shown in Figure 2b. The first designated RCS magnitude region (i.e., for logic bit-0) is from 0 to -38.5 dBsm. The second designated RCS magnitude region (i.e., for logic bit-1) is from -41.5 dBsm to $-\infty$, whereas the middle region of 3-dB separation from -38.5 to -41.5 dBsm has been designated for an invalid bit reading, i.e., a false logic bit.

The proposed tag is being designed to store a 32-bit digital ID code, therefore, variable $N = 32$. To realize a 32-bit code of any value, an RCS resonance or an RCS maximum must be produced at designated regions introduced in Figure 2a,b. For example, if a logical bit-1 is desired at any bit slot, an RCS resonance will have to be produced at the central frequency of that particular bit slot. A central frequency is located at +75 MHz from the start frequency of any bit slot. Similarly, if a logical bit-0 is desired at any bit-slot, an RCS maximum will have to be produced at the central frequency of that particular bit slot. Furthermore, an RCS maximum or minimum (i.e., an RCS resonance) must also have a magnitude that falls within the designated RCS region identified in Figure 2b. The above-outlined bit-identification process can be summarized as laid out in Table 1.

Table 1. Summary of bit decoding process.

Case	Frequency Range, f (GHz)	RCS Magnitude Range (dBsm)	Decoded Logic
1	$F_{a_N} < f < F_{b_N}$	$ RCS > -38.5$	0
2	$F_{a_N} < f < F_{b_N}$	$ RCS < -41.5$	1
3	$F_{a_N} < f < F_{b_N}$	$-38.5 > RCS > -41.5$	invalid
4	$F_{a_{N-1}} < f < F_{a_N}$	$RCS > 0$	invalid

To create a particular tag ID, the central frequencies ‘ f_c ’ of each bit slot is noted against the required 32-bit number. The length of each arc is calculated using the following formula [36]:

$$L_N = \frac{c}{2f} \sqrt{\frac{2}{\epsilon_r + 1}} \quad (1)$$

Once length of each arc has been calculated, its copper footprint is laid upon the substrate by using the following standard arc length formula:

$$L_N = R_N \cdot \theta_N \quad (2)$$

where R_N is the radius of arc with length L_N , and θ_N is its finishing angle in radians. It should be noted here that the starting angle for all the arc lengths is 0° .

2.2. Single-Bit Resonator

To verify the effect of arc length over RCS, a single element tag is simulated. The parametric analysis of a single bit resonator is shown in Figure 3, in which the inset shows the geometric shape of the arc on a tag. It should be noted here that according to Equation (2), the arc length is directly proportional to the arc’s subtended angle. Therefore, the RCS is plotted for various arc angles in Figure 3.

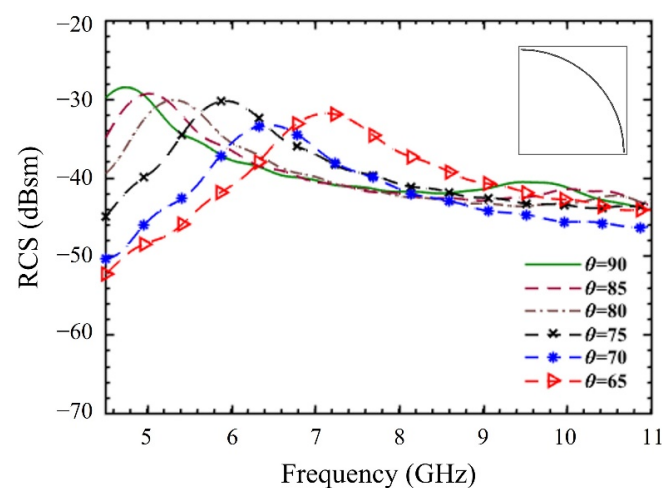


Figure 3. Effect of arc length over a single bit resonator.

It can be clearly observed that as the length of the arc is varied (by changing θ), the RCS maximum shifts along the frequency axis. Consequently, it can be concluded that the RCS maximum is controlled by variations in length L (or angle θ) of the arc. Contrary to this, an absence of an arc element will result in an RCS minimum. The RCS minimum in this manuscript will be called an ‘‘RCS resonance’’. In the proposed design, the width ‘ w ’ and gap ‘ g ’ between the arc elements have been chosen to be 0.2 mm.

The RCS for single arc length copper strip depicted in Figure 3 is spread out wide around its maxima. This indicates low Q for the resonator, which has an advantage of high RCS magnitude. An excellent and detailed discussion about the relationship between RCS, resonance frequency, and quality factor using Characteristic Mode Theory (CMT) can be found in [37].

2.3. Tag Instances

Multiple tag instances of the theoretical design shown in Figure 1 have been simulated to show that any 32-bit ID can be realized. Keeping brevity, a list of only three tag names along with their 32-bit ID’s is shown in Table 2.

Table 2. List of tags and their IDs.

Sr. No.	Tag Name	Tag 32-Bit ID
1	Tag 1	00011111111100111001001011000110
2	Tag 2	00101010100001010010010010010010
3	Tag 3	00100110010100000110100101000110

The first tag in the series, i.e., Tag 1, has been designed with an overall dimension of $17.9 \times 17.9 \text{ mm}^2$. The track width $w = 0.2 \text{ mm}$, and the first element has been placed at a position where its radius $R_1 = 7.2 \text{ mm}$. The subsequent arc elements are placed at a distance $g = 0.2 \text{ mm}$ apart. The rest of the radii can therefore be calculated as follows:

$$R_N = g + R_{N-1} \quad (3)$$

where $R_N \neq 1$.

It has been found through simulation that a total of 24 arc elements were sufficient to generate the 32-bit ID mentioned in Table 2, against Tag 1. An extra arc at a distance $g = 0.3 \text{ mm}$ has been placed to balance the coupling effect between the rest of the arc elements. The resulting tag geometry and its RCS response is shown in Figure 4.

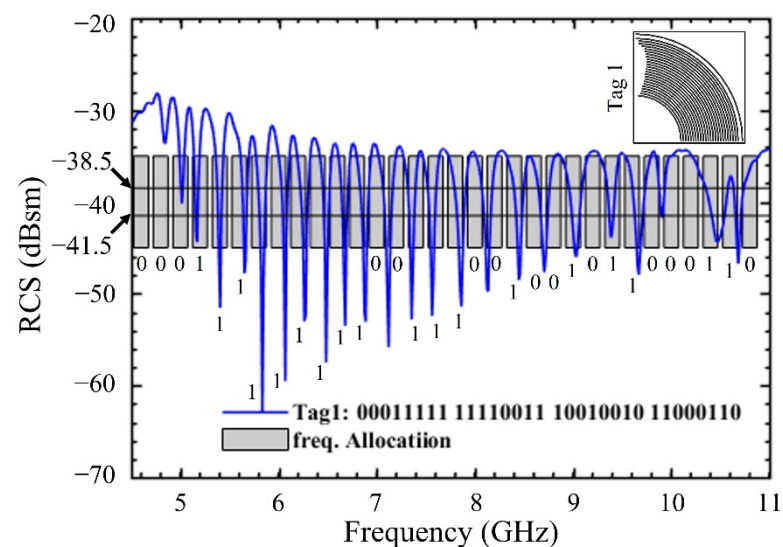


Figure 4. Simulated RCS response of Tag 1.

The bit values against each bit slot have been properly labeled according to the criterion set in Table 1. The most significant is at the lowest frequency of 4.55 GHz, whereas the least significant bit occurs at the highest frequency of 10.8 GHz. Frequency allocation as well as the RCS threshold regions have been shown in Figure 4 with a grayed rectangle and black dashed lines. A complete list of optimized arc lengths L1–L25 is given in Table 3.

Table 3. List of optimized parameters for Tag 1.

Parameter	L1	L2	L3	L4	L5
Value (mm)	11.22	11.45	11.98	12.5	13.03
Parameter	L6	L7	L8	L9	L10
Value (mm)	13.46	13.98	14.56	15.14	15.72
Parameter	L11	L12	L13	L14	L15
Value (mm)	16.3	16.82	17.4	18.01	18.6
Parameter	L16	L17	L18	L19	L20
Value (mm)	19.21	19.97	20.6	21.43	22.05
Parameter	L21	L22	L23	L24	L25
Value (mm)	23.18	24.31	24.94	26.07	27.17

The code density of the proposed tag is 9.98 bits/cm² and a spectral efficiency of 5 bits/GHz. These values will remain valid for all the rest of tag instances. The remaining two tag instances outlined in Table 2 (i.e., Tag 2 and Tag 3) have also been simulated and are shown in Figure 5 along with their RCS responses. All these tags encode 32-bit IDs, however the number of elements used in each tag is different. For example, Tag 2 has 13 and Tag 3 has 18 arc elements, respectively. The dimensions of these tags remain the same, and hence their code densities, as well as spectral efficiencies, are unchanged to that of Tag 1. Some of state-of-the-artwork has been compared with this work and highlighted in Table 4.

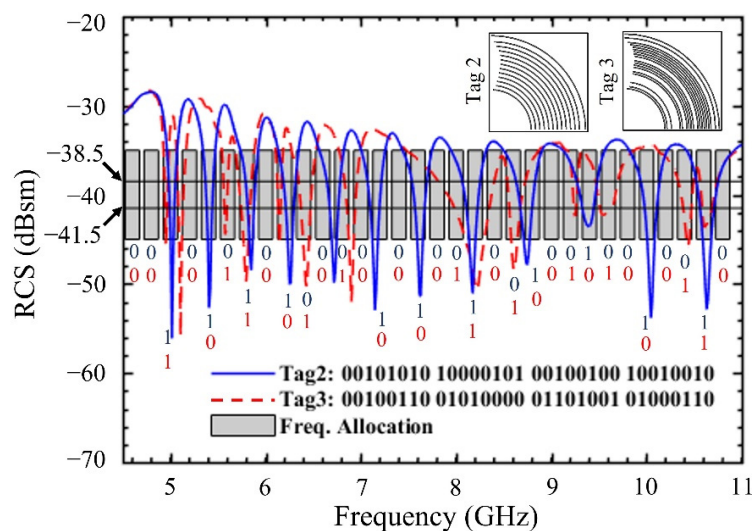


Figure 5. Simulated RCS response of CRFID tag instances: Tag 2, Tag 3. (Inset shows corresponding tag geometry).

Table 4. Comparison with state-of-the-art CRFID tags.

Ref. No.	Operating Frequency (GHz)	No. of Bits	Code Density (Bits/cm ²)	Spectral Efficiency (Bits/GHz)
[29]	2–3.6	20	1.77	12.5
[30]	6–13	8	3.26	1.14
[33]	2.2–3.5	20	0.6	15.4
[34]	4.5–7.5	14	5.88	4.66
[35]	2–8	8	10.74	1.33
Proposed	4.5–10.9	32	9.98	5

3. Fabrication and Measurement Results

All three tags have been fabricated on an ultra-thin 0.127 mm Roger's substrate, using standard PCB process. All tag instances were measured for RCS response in an anechoic chamber to verify the simulated response of the tag. The photographs of the fabricated tags are shown in Figure 6. A schematic of the measurement topology is shown in Figure 7a. The actual measurement setup in bi-static configuration in an anechoic chamber is shown in Figure 7.

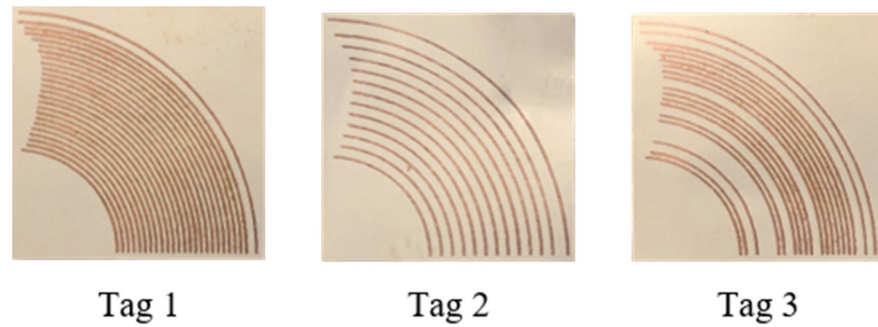


Figure 6. Photograph of fabricated CRFID tag instances.

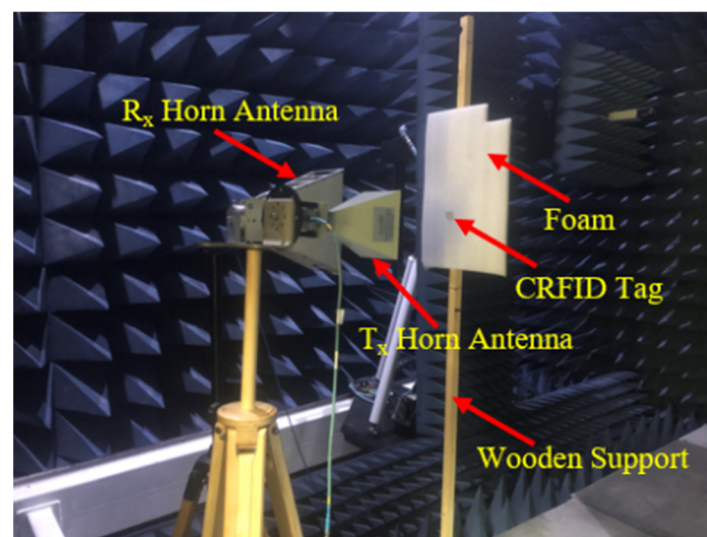
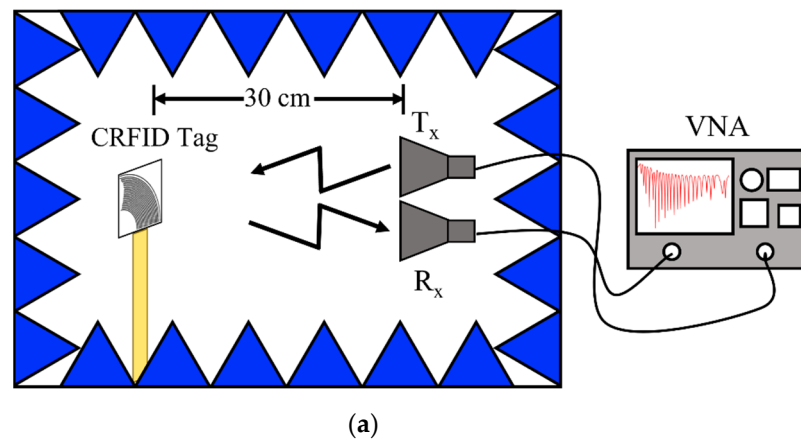


Figure 7. Measurement setup: (a) Schematic diagram; (b) Photograph of the measurement setup.

The RCS of fabricated tags was measured using a standard formula provided by [38], which is as follows:

$$\sigma^{\text{tag}} = \left[\frac{S_{21}^{\text{tag}} - S_{21}^{\text{isolation}}}{S_{21}^{\text{ref}} - S_{21}^{\text{isolation}}} \right]^2 \cdot \sigma^{\text{ref}} \quad (4)$$

where S_{21}^{tag} is measured S21 of the proposed tags, S_{21}^{ref} is the measured S-parameter of the reference rectangular metallic plate, $S_{21}^{\text{isolation}}$ is the isolation measurement without the tag, σ^{ref} is the known RCS value of the reference rectangular metallic plate, and σ^{tag} is the obtained RCS value of the proposed chipless RFID tag.

The experimentation to measure RCS response of the tags is performed using three different linearly polarized standard gain antennas (SGAs): (1) 3.95–5.85 GHz, (2) 5.85–8.20 GHz, and (3) 8.20–12.4 GHz. The SGAs are used in transmitting (Tx) mode and a broadband horn antenna (from 2–18 GHz) is used in the receiving (Rx) mode. The distance between the Tx and Rx antennas is kept around 0.75 m, which falls in the far-field region. The wideband horn and SGAs are connected to an Anritsu vector network analyzer (VNA) MS46122B. The SGAs have a gain of 12 dBi and the power delivered by VNA is 3 dBm. The simulated and measured RCS response of the Tag 1 is shown in Figure 8. Similarly, simulated, and measured RCS response of Tag 2–3 are shown in Figure 9. The measured results show a good correlation with those simulated.

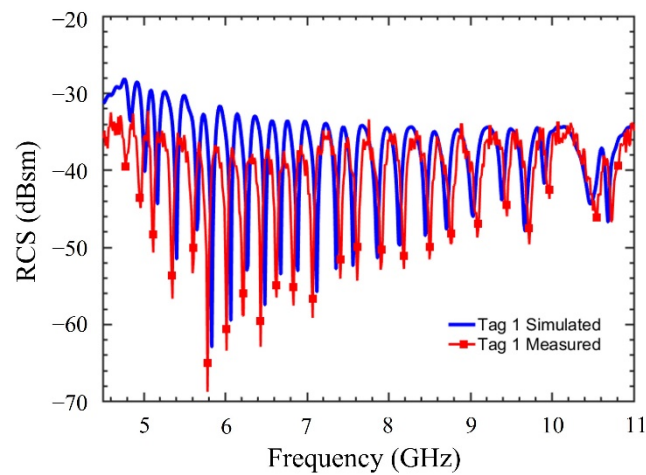


Figure 8. Measured and simulated RCS response of tag instance Tag 1.

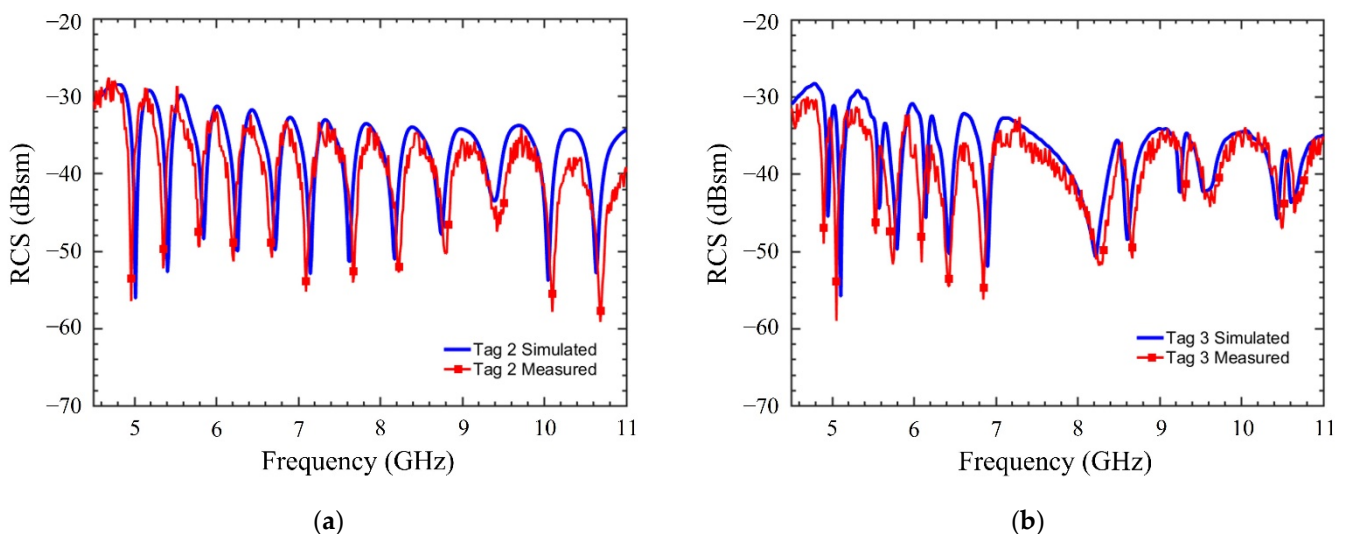


Figure 9. Measured and simulated RCS response of CRFID tag instances: (a) Tag 2; (b) Tag 3.

4. Conclusions

A unique chipless RFID tag was introduced and analyzed in this paper. The tag consists of curved metallic resonating elements of various lengths that provide resonant points on RCS plot. This results in a tag which can encode a 32-bit digital number, operating in 4.5–10.9 GHz band. A special frequency domain coding method was also proposed that can potentially lead to an efficient decoding of the information stored in tag's EM signature. The simulated and measured results show a stable RCS response with a code density of 9.98 bits/cm² and spectral efficiency of 5 bits/GHz. The tag was built on an ultra-thin 0.127 mm Roger's substrate. This unique tag is deemed very suitable for future product identification and IoT systems designed with chipless RFID tags capabilities.

Author Contributions: M.N., U.A.H. and H.U. designed, simulated, and fabricated the prototypes. They also performed the measurements and wrote the manuscript. F.A.T. conceived the idea, supervised the whole work, and revised the draft. H.R. and A.I.N. contributed to the concept, analyzed the results, and interpreted the data. All authors have read and agreed to the published version of the manuscript.

Funding: This project was funded in part by the Deanship of Scientific Research (DSR), King Abdulaziz University, Jeddah, Saudi Arabia, under grant no. DF-508-135-1441.

Institutional Review Board Statement: Not applicable.

Informed Consent Statement: Not applicable.

Data Availability Statement: Not applicable.

Acknowledgments: The authors are pleased to acknowledge the technical and financial support from the DSR, King Abdulaziz University, Jeddah, Saudi Arabia.

Conflicts of Interest: The authors declare no conflict of interest.

References

1. Preradovic, S.; Karmakar, N.C. Chipless RFID: Bar code of the future. *IEEE Microw. Mag.* **2010**, *11*, 87–97. [[CrossRef](#)]
2. Rezaiesarlak, R.; Manteghi, M. *Chipless RFID: Design Procedure and Detection Techniques*; Springer: Berlin/Heidelberg, Germany, 2016.
3. Khan, M.M.; Tahir, F.A.; Farooqui, M.F.; Shamim, A.; Cheema, H.M. 3.56-bits/cm² Compact Inkjet Printed and Application Specific Chipless RFID Tag. *IEEE Antennas Wirel. Propag. Lett.* **2016**, *15*, 1109–1112. [[CrossRef](#)]
4. Nguyen, D.H.; Zomorodi, M.; Karmakar, N.C. Spatial-Based Chipless RFID System. *IEEE J. Radio Freq. Ident.* **2019**, *3*, 46–55. [[CrossRef](#)]
5. Pöpperl, M.; Parr, A.; Mandel, C.; Jakoby, R.; Vossiek, M. Potential and practical limits of time-domain reflectometry chipless RFID. *IEEE Trans. Microw. Theory Tech.* **2016**, *64*, 2968–2976. [[CrossRef](#)]
6. Kalansuriya, P.; Karmakar, N.C.; Viterbo, E. On the detection of frequency-spectra-based chipless RFID using UWB impulsive interrogation. *IEEE Trans. Microw. Theory Tech.* **2012**, *60*, 4187–4197. [[CrossRef](#)]
7. Kofman, S.; Meerfeld, Y.; Sandler, M.; Dukler, S.; Alchanatis, V. Radio Frequency Identification System and Data Reading Method. U.S. Patent No. 8,167,212, 1 May 2012.
8. Feng, C.; Zhang, W.; Li, L.; Han, L.; Chen, X.; Ma, R. Angle-based chipless RFID tag with high capacity and insensitivity to polarization. *IEEE Trans. Antennas Propag.* **2015**, *63*, 1789–1797. [[CrossRef](#)]
9. Plessky, V.; Reindl, L. Review on SAW RFID Tags. *IEEE Trans. Ultrason. Ferroelect. Freq. Control* **2010**, *57*, 654–668. [[CrossRef](#)] [[PubMed](#)]
10. Jabeen, S.; Ullah, H.; Tahir, F.A. A 26 Bit Alternating U-shaped Chipless RFID Tag Using Slot Length Variation Technique. In Proceedings of the International Conference on Microwave, Antennas and Circuits, Islamabad, Pakistan, 21–22 December 2021; pp. 1–3.
11. Khan, M.M.; Tahir, F.A.; Cheema, H.M. Frequency Band Utilization Enhancement for Chipless RFID Tag through Place Value Encoding. In Proceedings of the IEEE International Antennas and Propagation Symposium and USNC-URSI Radio Science Meeting, Fajardo, PR, USA, 26 June–1 July 2016; pp. 1477–1478.
12. Khan, M.M.; Tahir, F.A.; Cheema, H.M. High Capacity Polarization Sensitive Chipless RFID Tag. In Proceedings of the IEEE International Antennas and Propagation Symposium and USNC-URSI Radio Science Meeting, Vancouver, BC, Canada, 19–24 July 2015; pp. 1770–1771.
13. Islam, M.A.; Karmakar, N.C. Compact Printable Chipless RFID Systems. *IEEE Trans. Microw. Theory Tech.* **2015**, *63*, 3785–3793. [[CrossRef](#)]

14. Wang, L.; Liu, T.; Sidénn, J.; Wang, G. Design of chipless RFID tag by using miniaturized open-loop resonators. *IEEE Trans. Antennas Propag.* **2018**, *66*, 618–626. [[CrossRef](#)]
15. Islam, M.A.; Karmakar, N.C. A novel compact printable dualpolarized chipless RFID system. *IEEE Trans. Microw. Theory Tech.* **2012**, *60*, 2142–2151. [[CrossRef](#)]
16. Chen, N.; Shen, Y.; Dong, G.; Hu, S. Compact scalable modeling of chipless RFID tag based on high-impedance surface. *IEEE Trans. Electron Dev.* **2019**, *66*, 200–206. [[CrossRef](#)]
17. Betancourt, D.; Haase, K.; Hübler, A.; Ellinger, F. Bending and folding effect study of—Exible fully printed and late-stage codi—Ed octagonal chipless RFID tags. *IEEE Trans. Antennas Propag.* **2016**, *64*, 2815–2823. [[CrossRef](#)]
18. Rmili, H.; Boularess, O.; Youssef, J.; Hakim, B.; Mittra, R.; Aguilu, T.; Tedjini, S. Robust detection for chipless RFID tags based on compact printable alphabets. *Sensors* **2019**, *19*, 4785. [[CrossRef](#)] [[PubMed](#)]
19. Marindra, A.M.J.; Tian, G.Y. Chipless RFID sensor tag for metal crack detection and characterization. *IEEE Trans. Microw. Theory Tech.* **2018**, *66*, 2452–2462. [[CrossRef](#)]
20. Haider, U.A.; Noman, M.; Ullah, H.; Tahir, F.A. A Compact L-Shaped 16 Bit Polarization Independent Chipless RFID Tag. In Proceedings of the 2020 International Conference on UK-China Emerging Technologies (UCET), Glasgow, UK, 20–21 August 2020; pp. 1–3.
21. Haider, U.A.; Noman, M.; Ullah, H.; Tahir, F.A. A Compact Chip-less RFID Tag for IoT Applications. In Proceedings of the 2020 IEEE International Symposium on Antennas and Propagation and North American Radio Science Meeting, Montreal, QC, Canada, 5–10 July 2020; pp. 1449–1450.
22. Zafar, S.; Rubab, S.; Ullah, H.; Tahir, F.A. A 12-bit Hexagonal Chip-less Tag for Radio Frequency Identification Applications. In Proceedings of the 2020 IEEE International Symposium on Antennas and Propagation and North American Radio Science Meeting, Montreal, QC, Canada, 5–10 July 2020; pp. 1503–1504.
23. Jabeen, I.; Ejaz, A.; Riaz, M.A.; Khan, M.J.; Akram, A.; Amin, Y.; Tenhunen, H. Miniaturized Elliptical Slot Based Chipless RFID Tag for Moisture Sensing. *Appl. Comput. Electromagn. Soc. J.* **2019**, *34*, 1366–1372.
24. Tariq, N.; Riaz, M.; Shahid, H.; Khan, M.; Khan, M.; Amin, Y.; Loo, J.; Tenhunen, H. Orientation Independent Chipless RFID Tag Using Novel Trefoil Resonators. *IEEE Access* **2019**, *7*, 122398–122407. [[CrossRef](#)]
25. Riaz, M.; Abdullah, Y.; Shahid, H.; Amin, Y.; Akram, A.; Tenhunen, H. Novel butterfly slot based chipless RFID tag. *Radioengineering* **2018**, *27*, 776–783. [[CrossRef](#)]
26. Tariq, N.; Riaz, M.; Shahid, H.; Khan, M.; Tenhunen, H. A Novel Kite-Shaped Chipless RFID Tag for Low-Profile Applications. *IETE J. Res.* **2019**, 1–8. [[CrossRef](#)]
27. Sharma, V.; Malhotra, S.; Hashmi, M. Slot Resonator Based Novel Orientation Independent Chipless RFID Tag Configurations. *IEEE Sens. J.* **2019**, *19*, 5153–5160. [[CrossRef](#)]
28. Jabeen, I.; Ejaz, A.; Rahman, M.; Naghshvarianjahromi, M.; Khan, M.; Amin, Y.; Tenhunen, H. Data-Dense and Miniature Chipless Moisture Sensor RFID Tag for Internet of Things. *Electronics* **2019**, *8*, 1182. [[CrossRef](#)]
29. Havlicek, J.; Švanda, M.; Polivka, M.; Machac, J.; Kracek, J. Chipless RFID Tag Based on Electrically Small Spiral Capacitively Loaded Dipole. *IEEE Antennas Wirel. Propag. Lett.* **2017**, *16*, 3051–3054. [[CrossRef](#)]
30. Islam, M.A.; Yap, Y.; Karmakar, N.C.; Azad, A. Compact Printable Orientation Independent Chipless RFID Tag. *Prog. Electromagn. Res. C* **2012**, *33*, 55–66. [[CrossRef](#)]
31. Abdulkawi, W.M.; Sheta, A.A. High coding capacity chipless radiofrequency identification tags. *Microw. Opt. Technol. Lett.* **2019**, *62*, 592–599. [[CrossRef](#)]
32. Ma, Z.; Jiang, Y. High-Density 3D Printable Chipless RFID Tag with Structure of Passive Slot Rings. *Sensors* **2019**, *19*, 2535. [[CrossRef](#)] [[PubMed](#)]
33. Svanda, M.; Polivka, M.; Havlicek, J.; Machac, J.; Werner, D.H. Platform Tolerant, High Encoding Capacity Dipole Array-Plate Chipless RFID Tags. *IEEE Access* **2019**, *7*, 138707–138720. [[CrossRef](#)]
34. Babaeian, F.; Karmakar, N. Compact Multi-Band Chipless RFID Resonators for Identification and Authentication Applications. *Electron. Lett.* **2020**, *56*, 724–727. [[CrossRef](#)]
35. Salemi, F.; Hassani, H.R.; Mohammad-Ali-Nezhad, S. Linearly Polarized Compact Extended U-shaped Chipless RFID Tag. *AEU-Int. J. Electron. Commun.* **2020**, *117*, 153129. [[CrossRef](#)]
36. Dissanayake, T.; Esselle, K.P. Prediction of the notch frequency of slot loaded printed UWB antennas. *IEEE Trans. Antennas Propag.* **2007**, *55*, 3320–3325. [[CrossRef](#)]
37. Rezaiesarlak, R.; Manteghi, M. Design of Chipless RFID Tags Based on Characteristic Mode Theory (CMT). *IEEE Trans. Antennas Propag.* **2015**, *63*, 711–718. [[CrossRef](#)]
38. Vena, A.; Perret, E.; Tedjini, S. Chipless RFID Tag Using Hybrid Coding Technique. *IEEE Trans. Microw. Theory Tech.* **2011**, *59*, 3356–3364. [[CrossRef](#)]